Journal of Computational Physics **178,** 307–322 (2002)
doi:10.1006/jcph.2002.7022, available online at http://www.idealibrary.com on IDEAL®

Entropy Splitting for High-Order Numerical Simulation of Compressible Turbulence

N. D. Sandham,* Q. Li,* and H. C. Yee†

*Aeronautics and Astronautics, School of Engineering Sciences, University of Southampton, Southampton SO17 1BJ, United Kingdom; and †NASA Ames Research Center, Moffett Field, California 94035

Received August 28, 2001; revised February 6, 2002

A stable high-order numerical scheme for direct numerical simulation (DNS) of shock-free compressible turbulence is presented. The method is applicable to general geometries. It contains no upwinding, artificial dissipation, or filtering. Instead the method relies on the stabilizing mechanisms of an appropriate conditioning of the governing equations and the use of compatible spatial difference operators for the interior points (interior scheme) as well as the boundary points (boundary scheme). An entropy-splitting approach splits the inviscid flux derivatives into conservative and nonconservative portions. The spatial difference operators satisfy a summation-by-parts condition, leading to a stable scheme (combined interior and boundary schemes) for the initial boundary value problem using a generalized energy estimate. A Laplacian formulation of the viscous and heat conduction terms on the right hand side of the Navier–Stokes equations is used to ensure that any tendency to odd–even decoupling associated with central schemes can be countered by the fluid viscosity. The resulting methods are able to minimize the spurious high-frequency oscillations associated with pure central schemes, especially for long time integration applications such as DNS. For validation purposes, the methods are tested in a DNS of compressible turbulent plane channel flow at low values of friction Mach number, where reference turbulence data bases exist. It is demonstrated that the methods are robust in terms of grid resolution, and in good agreement with published channel data. Accurate turbulence statistics can be obtained with moderate grid sizes. Stability limits on the range of the splitting parameter are determined from numerical tests.

1. INTRODUCTION

This work forms part of a larger research project to develop efficient low-dissipative high-order numerical techniques for high-speed turbulent flow simulation for general geometries, including shock wave interactions with turbulence. The requirements on a numerical method are stringent. For turbulence, the method must be capable of resolving accurately a wide

0021-9991/02 $35.00

range of length scales, while for shock waves the method must be stable and not generate excessive local oscillations. Classical methods are either too dissipative, incapable of handling complex geometries, or incapable of shock capturing. Higher order ENO, WENO, or hybrid schemes are too expensive for practical turbulent flow simulation. Previous work of Yee *et al*. [1] and Sjögreen and Yee [2] developed efficient high-order shock-capturing schemes which minimize the use of numerical dissipation away from shock waves. Recent work of Yee and Sjögreen [3] has proposed an approach to determine the appropriate amount of numerical dissipation/filtering for use with high-order schemes. This includes the switching and/or blending from one kind of filter to another, as discussed in Yee *et al*. [5]. The desired property of this approach is to construct sensors that are able to distinguish shock waves from turbulent fluctuations and spurious high-frequency oscillations to further improve the stability and accuracy of direct numerical simulation (DNS) and large-eddy simulation (LES). The objective of the present study is to add new techniques to these methods so that the use of numerical dissipation can be minimized for shock-free compressible turbulent flow simulations.

For the past two decades, the methods of choice for turbulence simulation have been spectral if geometries were simple, or high-order nondissipative finite differences or spectral elements if the geometries were complex. With the advent of massively parallel computing and the need for ease and efficiency of parallelization there has been some use of second-order methods for turbulence simulation. These second-order methods usually require very fine grids and correspondingly small time steps to counterbalance the low-order accuracy of the schemes. Hence, stable highly parallelizable high-order methods would be preferred. Here we focus on high-order noncompact and compact nondissipative central spatial differencing with orders of accuracy that are fourth order or higher. The usual methods of improving nonlinear stability of such methods without resorting to extreme grid refinement have been the use of filters or added numerical dissipation. For slowly developing long time integration problems such as DNS of turbulent flows, the added numerical dissipation leads to undesirable amplitude errors and hence inaccurate turbulence structures and statistics. In order to minimize the use of numerical dissipation, what is more important, we believe, is first to condition the compressible Navier–Stokes equations so that they have certain nonlinear stability properties, including the physical boundaries. Second, for robust methods, we need to construct high-order schemes that have a discrete analogue of the conditioned governing equations, including stable high-order numerical boundary condition treatments. Olsson and Oliger [6] and Gerritsen and Olsson [7] have developed such a theory for the perfect gas compressible Euler equations using high-order central differencing. Their theory has led to a splitting of the inviscid flux derivatives of the governing equations, hereafter referred to as "entropy splitting." Yee *et al*. [5] and Vinokur and Yee [8] viewed this splitting as a conditioned form of the original conservation laws and performed studies on 2D problems with periodic and nonperiodic physical boundary conditions. They also extended the splitting to a thermally perfect gas and 3D curvilinear moving grids. Their results indicate that the splitting can in general improve nonlinear stability and minimize the use of numerical dissipation for smooth flows and for problems containing complex shock-turbulence interactions. They also showed that entropy splitting can minimize the generation of high-frequency oscillation producing nonlinear instability. Such stability properties are of much value in the context of turbulence simulation.

With the aforementioned techniques, in conjunction with a Laplacian formulation of the viscous and heat conduction terms, we aim to demonstrate that very accurate turbulence

statistics can be obtained with moderate grid sizes for a 3D compressible channel flow. We note that the chosen test case is for validation and comparison purposes and that the method of choice for this low Mach number and Reynolds number and simple geometry problem may well still be the spectral method.

2. ENTROPY SPLITTING AND SUMMATION-BY-PARTS APPROACH

In this section and the next we focus on a reformulation of the Navier–Stokes equations. For the subset of these equations that constitutes the Euler equations of gas dynamics we use an entropy-splitting approach. For the remaining terms a Laplacian portion is always included. We confine the discussion to a thermally perfect gas with constant specific heats

$$p = \rho RT, \tag{1}$$

$$e = c_v T, \tag{2}$$

where p is the pressure, ρ the density, T the temperature, and e the specific internal energy, with R the gas constant and c_v the specific heat at constant volume. Yee *et al*. [5] and Vinokur and Yee [8] present an extended formulation for a gas that is only thermally perfect (with internal energy an arbitrary function of temperature) and for curvilinear moving grids.

2.1. Split Form of Conservation Laws

Olsson and Oliger [6] and references cited therein give a detailed derivation of the entropy-splitting procedure. Here we briefly review their procedure for the system of symmetrizable hyperbolic conservation laws

$$u_t + f_x = 0, \tag{3}$$

where u and f are column vectors. This system can be transformed by an entropy vector w

$$u_w w_t + f_w w_x = 0, \tag{4}$$

where the Jacobian matrices u_w and f_w are symmetric, u_w is positive definite, and $u(w)$ and $f(w)$ are homogeneous of degree β. Thus we can write a split form of the original system as

$$\frac{\beta}{\beta+1}u_t + \frac{1}{\beta+1}u_w w_t + \frac{\beta}{\beta+1}f_x + \frac{1}{\beta+1}f_w w_x = 0, \quad \beta \neq -1, \tag{5}$$

with β a splitting parameter ($\beta \to \infty$ recovers the original conservative form). The homogeneity conditions

$$u(\theta w) = \theta^\beta u(w), \tag{6}$$

$$f(\theta w) = \theta^\beta f(w), \tag{7}$$

with θ a constant, lead to $u_w w = \beta u$ and $f_w w = \beta f$, respectively. This enables us to use integration by parts over, for example, a space domain $x = x_0$ to $x = x_1$ to rewrite the split

form of the equations in terms of the time derivative of an inner product

$$\frac{d}{dt}(w, u_w w) = -[w^T f_w w]_{x_0}^{x_1}. \tag{8}$$

Olsson and Oliger go on to write a "generalized" energy estimate for the norm defined by the left hand side of this equation. The existence of this norm based on the split form for the Euler equations is presented in Gerritsen and Olsson [7].

2.2. Entropy Split Form of Euler Equations

For a perfect gas, a suitable transformed vector of variables W for the Euler equations with the usual conservative vector U can be found by defining

$$W = \frac{\partial \eta}{\partial U}, \tag{9}$$

where $\eta = \rho h(S)$ is an entropy function and $h(S)$ is an arbitrary but differentiable function of $S = \ln(p\rho^{-\gamma})$, which is the physical entropy nondimensionalized by c_v and with a suitably defined datum. The choice of $h(S)$ is restricted by the homogeneity requirement and a positive definite condition on $U_W = \partial U/\partial W$. One solution is

$$h(S) = \beta \exp\left(\frac{S}{(1-\gamma)\beta}\right). \tag{10}$$

For a full derivation of this formulation see Harten [9] and Gerritsen and Olsson [7].

The Euler equations, which would normally be written in the usual notation as

$$U_t + F_x + G_y + H_z = 0, \tag{11}$$

with

$$U = \begin{bmatrix} \rho \\ \rho u \\ \rho v \\ \rho w \\ E_T \end{bmatrix}, \quad F = \begin{bmatrix} \rho u \\ \rho u^2 + p \\ \rho uv \\ \rho uw \\ (E_T + p)u \end{bmatrix}, \quad G = \begin{bmatrix} \rho v \\ \rho uv \\ \rho v^2 + p \\ \rho vw \\ (E_T + p)v \end{bmatrix}, \quad H = \begin{bmatrix} \rho w \\ \rho uw \\ \rho vw \\ \rho w^2 + p \\ (E_T + p)w \end{bmatrix}, \tag{12}$$

and

$$E_T = \rho[e + (u^2 + v^2 + w^2)/2], \tag{13}$$

can now be rewritten in the entropy split form

$$\frac{\beta}{\beta+1}U_t + \frac{1}{\beta+1}U_W W_t + \frac{\beta}{\beta+1}(F_x + G_y + H_z) + \frac{1}{\beta+1}(F_W W_x + G_W W_y + H_W W_z) = 0 \tag{14}$$

(see Yee *et al*. [5] for the conditions on β). Here the transformed entropy vector W is

$$W = \frac{p^*}{p}\begin{bmatrix} E_T - 2\rho e - p(1+\beta) \\ -\rho u \\ -\rho v \\ -\rho w \\ \rho \end{bmatrix}, \tag{15}$$

where p^* is given by

$$p^* = -(p\rho^{-\gamma})^{\frac{1}{\beta(1-\gamma)}}. \tag{16}$$

The upper triangular parts of the symmetric matrices F_W, G_W, and H_W are given [5] by

$$F_W = \frac{1}{p^*}\begin{pmatrix} c_1\rho u & c_1\rho u^2 - p & c_1\rho uv & c_1\rho uw & u[c_1E_T + (c_2-1)p] \\ & u(c_1\rho u^2 - 3p) & v(c_1\rho u^2 - p) & w(c_1\rho u^2 - p) & u^2c_3 - (E_T+p)p/\rho \\ & & u(c_1\rho v^2 - p) & c_1\rho uvw & uv[c_1E_T + (c_2-2)p] \\ & & & u(c_1\rho w^2 - p) & uw[c_1E_T + (c_2-2)p] \\ & & & & uc_4 \end{pmatrix}, \tag{17}$$

$$G_W = \frac{1}{p^*}\begin{pmatrix} c_1\rho v & c_1\rho uv & c_1\rho v^2 - p & c_1\rho vw & v[c_1E_T + (c_2-1)p] \\ & v(c_1\rho u^2 - p) & u(c_1\rho v^2 - p) & c_1\rho uvw & uv[c_1E_T + (c_2-2)p] \\ & & v(c_1\rho v^2 - 3p) & w(c_1\rho v^2 - p) & v^2c_3 - (E_T+p)p/\rho \\ & & & v(c_1\rho w^2 - p) & vw[c_1E_T + (c_2-2)p] \\ & & & & vc_4 \end{pmatrix}, \tag{18}$$

$$H_W = \frac{1}{p^*}\begin{pmatrix} c_1\rho w & c_1\rho uw & c_1\rho vw & c_1\rho w^2 - p & w[c_1E_T + (c_2-1)p] \\ & w(c_1\rho u^2 - p) & c_1\rho uvw & u(c_1\rho w^2 - p) & uw[c_1E_T + (c_2-2)p] \\ & & w(c_1\rho v^2 - p) & v(c_1\rho w^2 - p) & vw[c_1E_T + (c_2-2)p] \\ & & & w(c_1\rho w^2 - 3p) & w^2c_3 - (E_T+p)p/\rho \\ & & & & wc_4 \end{pmatrix}, \tag{19}$$

where

$$c_1 = \frac{1-\beta(1-\gamma)}{\beta(1-\gamma)-\gamma}, \tag{20}$$

$$c_2 = \frac{1}{\beta(1-\gamma)-\gamma}, \tag{21}$$

$$c_3 = c_1E_T + (c_2-2)p, \tag{22}$$

$$c_4 = \frac{c_1E_T^2}{\rho} + p\left[2(c_2-1)\frac{E_T}{\rho} - q^2\right] + \frac{p^2}{\rho}[c_2(1+\beta)-2] \tag{23}$$

and

$$q^2 = u^2 + v^2 + w^2. \tag{24}$$

By using the definition of E_T, we obtain alternate forms of the above relations that do not contain E_T. Normally, we need to compute U_W for the split form of $U_t = \frac{\beta}{\beta+1}U_t + \frac{1}{\beta+1}U_W W_t$. However, we only consider a semidiscrete approach of applying temporal discretizations. Aside from using the split form of the inviscid flux derivatives F_x, G_y, and H_z, we do not have to use the split form of U_t for implementation. Thus the final form of the semidiscrete entropy-splitting approach still can be expressed in terms of conservative and primitive variables, making possible easy and efficient implementation to existing computer codes.

2.3. Summation by Parts

In the proof of the generalized energy estimate for entropy splitting use was made of integration by parts. To obtain a similar stable estimate in numerical simulation, for both the interior and boundary spatial schemes, we need difference operators that satisfy a discrete analogy of this, known as summation by parts (SBP). SBP operators first appeared in the work of Strand [10]. Stable boundary difference operators (boundary schemes) for central schemes (interior schemes) are discussed in Olsson [11] and known as the SBP projection method. These stable boundary operators were developed for the characteristic variables for systems of symmetrizable hyperbolic conservation laws. Carpenter *et al*. [12] developed a variant of the SBP boundary difference operators for the linear or linearized hyperbolic equations without the entropy-splitting concept. For the numerical experiment, we employ the Carpenter *et al*. boundary scheme. In his notation a first-derivative SBP operator for the combined interior and boundary scheme is given by

$$\mathbf{D}\vec{u} = \frac{1}{\hat{h}}\mathbf{P}^{-1}\mathbf{Q}\vec{u}, \tag{25}$$

with a uniform grid spacing $\hat{h}$. For a fourth-order central interior scheme the matrices $\mathbf{P}$ and $\mathbf{Q}$ are given by

$$\mathbf{P} = \begin{pmatrix} \frac{-(216b+2160a-2125)}{12960} & \frac{81b+675a+415}{540} & \frac{-(72b+720a+445)}{1440} & \frac{-(108b+756a+421)}{1296} & & \\ \frac{(81b+675a+415)}{540} & \frac{-(4104b+32400a+11225)}{4320} & \frac{(1836b+14580a+7295)}{2160} & \frac{-(216b+2160a+655)}{4320} & & \\ \frac{-(72b+720a+445)}{1440} & \frac{(1836b+14580a+7295)}{2160} & \frac{-(4104b+32400a+12785)}{4320} & \frac{(81b+675a+335)}{540} & & \\ -\frac{(108b+756a+421)}{1296} & \frac{-(216b+2160a+655)}{4320} & \frac{(81b+675a+335)}{540} & \frac{-(216b+2160a-12085)}{12960} & & \\ & & & & 1 & \\ & & & & & \ddots \end{pmatrix}, \tag{26}$$

$$\mathbf{Q} = \begin{pmatrix} \frac{-1}{2} & \frac{-(864b+6480a+305)}{4320} & \frac{(216b+1620a+725)}{540} & \frac{-(864b+6480a+3335)}{4320} & & \\ \frac{(864b+6480a+305)}{4320} & 0 & \frac{-(864b+6480a+2315)}{1440} & \frac{(108b+810a+415)}{270} & & \\ \frac{-(216b+1620a+725)}{540} & \frac{(864b+6480a+2315)}{1440} & 0 & \frac{-(864b+6480a+785)}{4320} & \frac{-1}{12} & \\ \frac{(864b+6480a+3335)}{4320} & \frac{-(108b+810a+415)}{270} & \frac{(864b+6480a+785)}{4320} & 0 & \frac{2}{3} & \frac{-1}{12} \\ & & \frac{1}{12} & \frac{-2}{3} & 0 & \frac{2}{3} \\ & & & \ddots & \ddots & \ddots \end{pmatrix}, \tag{27}$$

where

$$a = \frac{-(2177\sqrt{295369} - 1166427)}{25488} \tag{28}$$

and

$$b = \frac{(66195\sqrt{53}\sqrt{5573} - 35909375)}{101952}. \tag{29}$$

The dots in Eqs. (26) and (27) indicate continuations of the previous line entries along matrix diagonals. The derivative operator $\mathbf{D}$ is then computed by inverting $\mathbf{P}$ and multiplying by $\mathbf{Q}$. This is done during initialization of the program to ensure that the elements of $\mathbf{D}$ are known to machine accuracy. In other words, the coefficients of the boundary scheme at the first four grids points $j = 1, 2, 3, 4$, with j the grid index in a chosen direction, are the form indicated on the first four rows of the above form.

For the second derivative, Carpenter proposes an analogous SBP criterion. For the fourth-order noncompact central interior scheme this leads to a form that can be written explicitly as

$$\mathbf{D^2} = \frac{1}{\hat{h}^2}\begin{pmatrix} \frac{35}{23} & -\frac{26}{3} & \frac{19}{2} & -\frac{14}{3} & \frac{11}{12} & \\ \frac{11}{12} & -\frac{5}{3} & \frac{1}{2} & \frac{1}{3} & -\frac{1}{12} & \\ -\frac{1}{12} & \frac{4}{3} & -\frac{5}{2} & \frac{4}{3} & -\frac{1}{12} & \\ & \cdot & \cdot & \cdot & \cdot & \cdot \\ & & \cdot & \cdot & \cdot & \cdot \\ & & & \cdot & \cdot & \cdot \end{pmatrix}. \tag{30}$$

Here $\mathbf{D^2}$ is not $\mathbf{D} \times \mathbf{D}$ of the first-derivative formula.

3. NAVIER–STOKES FORMULATION

By itself, entropy splitting and the compatible SBP boundary formulation might not be able to produce a robust method for the Navier–Stokes equations, and attention needs also to be focused on the viscous and heat conduction terms. For the momentum equations the viscous terms are commonly written as

$$\frac{\partial \tau_{ij}}{\partial x_j} = \frac{\partial}{\partial x_j}\left(\mu\left[\frac{\partial u_i}{\partial x_j} + \frac{\partial u_j}{\partial x_i}\right] - \frac{2}{3}\mu\left[\frac{\partial u_k}{\partial x_k}\right]\delta_{ij}\right), \tag{31}$$

with μ the dynamic viscosity. The equations contain derivatives of quantities that already contain derivatives. Two operations of a first derivative are not equal to a single second-derivative operator. For example, a second-order central differencing of a function f_x with $\hat{h}$ as the uniform grid spacing is

$$(f_x)_j \approx \frac{f_{j+1} - f_{j-1}}{2\hat{h}}. \tag{32}$$

Two operations of a first derivative give

$$((f_x)_x)_j \approx \frac{f_{j+2} - 2f_j + f_{j-2}}{4\hat{h}^2}, \tag{33}$$

which leads to odd–even decoupling, while a single second-derivative operator gives

$$(f_{xx})_j \approx \frac{f_{j+1} - 2f_j + f_{j-1}}{\hat{h}^2}, \tag{34}$$

which can lead to physical damping of $2\hat{h}$ oscillations.

In order to avoid odd–even decoupling from the outset we rewrite the viscous terms in what we call a Laplacian form:

$$\frac{\partial \tau_{ij}}{\partial x_j} = \mu \frac{\partial^2 u_i}{\partial x_j \partial x_j} + \frac{\mu}{3} \frac{\partial}{\partial x_i}\left(\frac{\partial u_k}{\partial x_k}\right) + \frac{\partial \mu}{\partial x_j}\left(\frac{\partial u_i}{\partial x_j} + \frac{\partial u_j}{\partial x_i}\right) - \frac{2}{3}\frac{\partial \mu}{\partial x_i}\frac{\partial u_j}{\partial x_j}. \tag{35}$$

The first term is a Laplacian, corresponding to the incompressible formulation of the equations. This term is always treated with second-derivative operators. The second term is zero in incompressible flow. The third term is zero if the viscosity is constant, and the last term is zero if either the viscosity is constant or the flow is incompressible.

The same procedure is applied to the energy equation leading to a first term containing the Laplacian of $\gamma e/Pr + u_i u_i/2$, where Pr is the Prandtl number. In a subsequent study, attempts have been made to reformulate the continuity equation in a similar way (Sandham and Yee [13]). However, these methods have not been proven to be robust in other flows and complicate the parallelization, so they are not pursued further here.

4. COMPRESSIBLE CHANNEL FLOW

As a test case for application of the method we consider wall-bounded isothermal compressible turbulent channel flow. The fluid mechanics of this problem have been studied in some detail by Coleman *et al*. [14] and Huang *et al*. [15]. They showed that the only compressibility effect at moderate Mach numbers comes from the variation of fluid properties with temperature. They used a uniform body force term

$$\Phi = -\frac{1}{\rho}\frac{\partial P}{\partial x} \tag{36}$$

to drive the flow but recommended a different constant pressure gradient approach, which involves splitting off a driving pressure gradient from the pressure terms in the x-momentum and energy equations. In the dimensionless x-momentum equation this leads to a forcing term on the right hand side given by

$$-\frac{\partial P}{\partial x} = 1, \tag{37}$$

while in the energy equation we have a corresponding term on the right hand side given by

$$-u\frac{\partial P}{\partial x} = u. \tag{38}$$

We present test cases using both formulations. For simplicity we solve the fixed body force or pressure gradient problem rather than constant mass flow rate. Thus the wall shear stress and mass flow rate vary during the simulation. In the next sections we present grid refinement studies and comparisons to published DNS databases, computed using spectral methods.

Channel half-width h, mean friction velocity u_τ, wall temperature, and bulk (integrated) density are the reference quantities for formulating dimensionless variables.

Sensitivity to the parameter β was also checked. The numerical experiments in [5] provide some guidance on the beneficial range of β. In general, the beneficial range of β becomes smaller as the speed of the flow increases, especially when shear and shock waves and vortices start to form. On the other hand, the bigger the $\beta \geq 100$, the less likely it is that there will be a benefit from the entropy splitting since it is closer to the unsplit situation. Depending on the speed of the flow and Reynolds number, for turbulence flows, instability usually occurs for β close to 1 (nearly 50% nonconservative portion of the governing equations is used) and for large β (nearly 100% unsplit). For a calculation on a grid $18 \times 61 \times 18$ the turbulent channel simulation was stable for $1.25 < \beta < 12$. The different βs within this range can lead to different turbulence statistics, for example measured by a momentum equation balance [18]. However, results for $\beta = 2$ and $\beta = 4$ were indistinguishable, and deviations only started to appear for $\beta \geq 8$. Consequently we used $\beta = 4$ for all of the simulations presented here. It was verified that the choice of β did not affect the converged (fine grid) results. The use of Mach and Reynolds numbers to adaptively determine the value of β at each grid point, as suggested in Yee and Sjögreen [3], appears to be a promising development and is the subject of current investigation.

5. GRID REFINEMENT STUDY

For a first study we take a simplified case in which the fluid properties (viscosity and conductivity) are held constant and the computational box size is kept small. The latter is justified as a method of reducing cost as the gross turbulence statistics are relatively insensitive to computation box size, so long as the domains are still significantly larger than the minimal domains on which turbulence can be sustained. A Mach number of 0.1 is chosen, based on mean friction velocity and sound speed corresponding to the fixed wall temperature. Together with the constant property assumption this choice of Mach number means that results can reasonably be compared to results from previous incompressible flow calculations. The computations were carried out at a fixed CFL = 2.0. They were started with artificial initial conditions and first run to time $t = 50$, by which time dependence on the initial conditions is lost. Statistics presented in this section were accumulated over the time interval $t = 200$–300.

We begin with a comparison of three simulations with grids $12 \times 41 \times 12$, $24 \times 81 \times 24$, and $36 \times 121 \times 36$. The largest number in each case corresponds to the direction normal to the wall (y). The computational box has nondimensional length 3 in the (streamwise) x-direction, 1.5 in the (spanwise) z-direction, and 2 in the y-direction. The x- and z-directions have periodic boundary conditions with uniform grid spacing. In the y-direction, the grid is stretched according to

$$\frac{y}{h} = \frac{\tanh(c_\eta \eta)}{\tanh c_\eta}, \tag{39}$$

with η uniformly distributed on $[-1, 1]$, $c_\eta = 1.7$. The ratio of grid points in each direction was chosen so that all directions have roughly the same degree of resolution of the relevant turbulence microscales in each direction. For these simulations, the classical fourth-order Runge–Kutta temporal discretization, and fourth-order noncompact (five-point) central

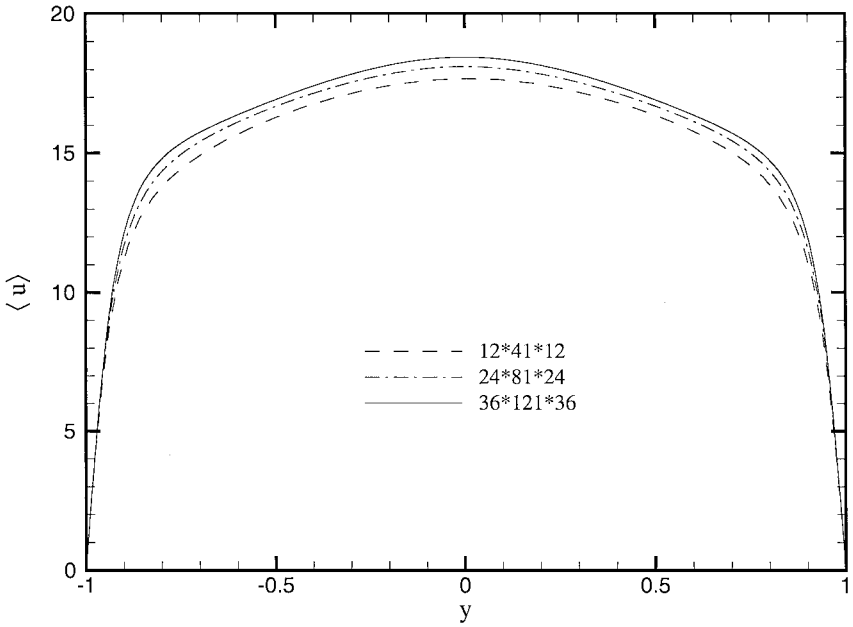

FIG. 1. Mean-velocity profiles.

spatial interior scheme together with the Carpenter *et al*. [12] boundary scheme have been used. Figure 1 shows the mean flow, Fig. 2 the root mean normal stresses, and Fig. 3 the stress profiles across the channel. Angle brackets ⟨⟩ denote averages over the homogeneous spatial directions and time while in the usual notation double primes denote deviations from

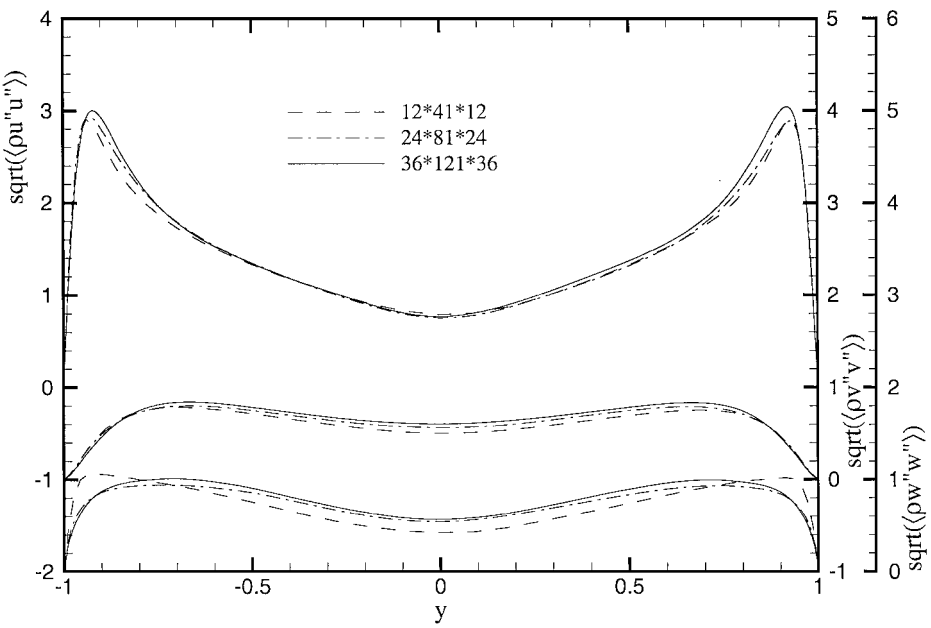

FIG. 2. Effect of grid refinement on normal stresses. The top curves relate to the left scale, the middle to the right scale, and the lowest to the furthest right scale.

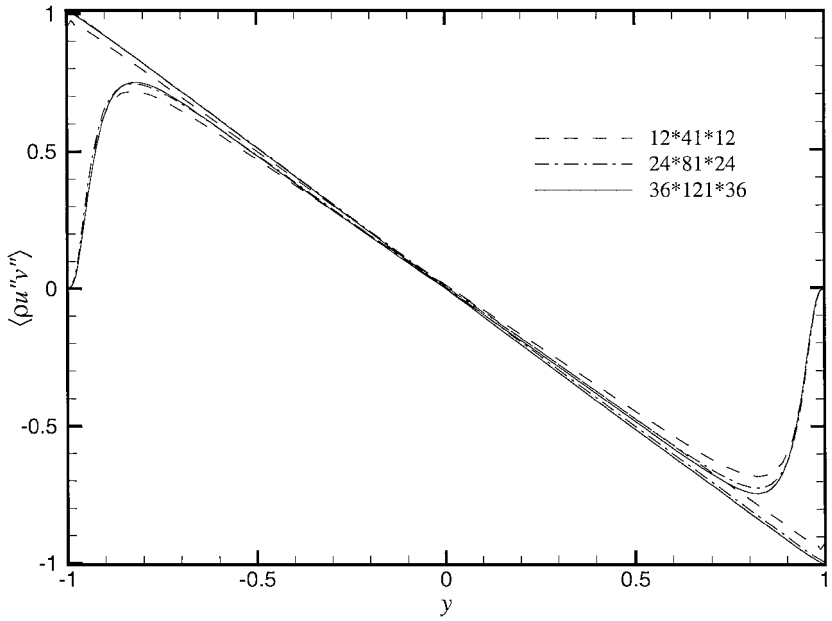

FIG. 3. Effect of grid refinement on turbulent shear stress (curve falling to zero at the walls). The total stress (straight lines, nonzero at walls) is also shown.

mass-weighted (Favre) averages. The convergence is not uniform across the channel but the change from medium to fine grid is smaller than the change from coarse to medium grid. A comparison of the rms quantities with an incompressible flow simulation on the same size computational box (Z. Hu, private communication) is shown in Fig. 4. Here we compare

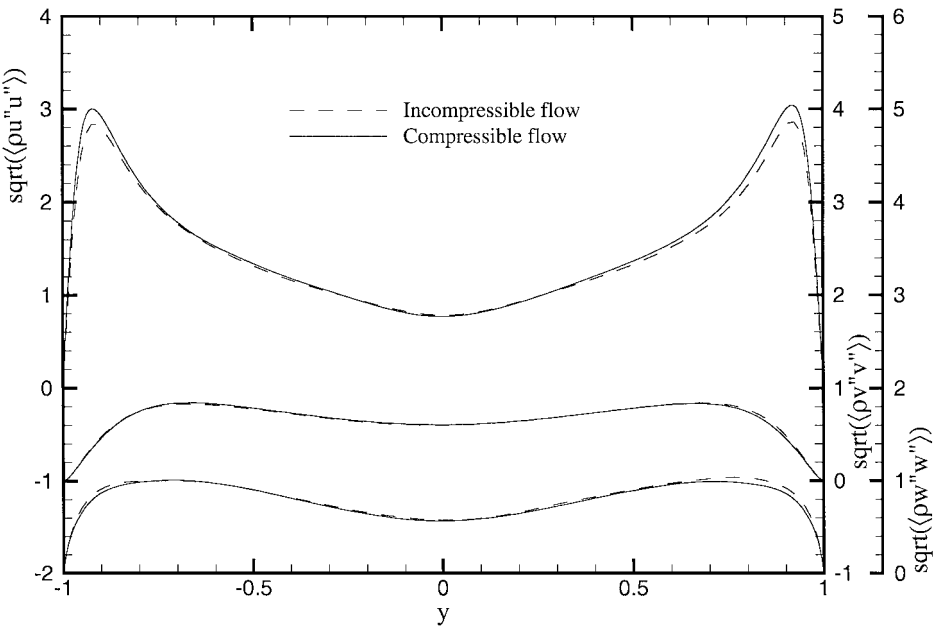

FIG. 4. Comparison of weighted turbulence quantities on a $36 \times 121 \times 36$ grid with an incompressible flow simulation on a $32 \times 32 \times 81$ grid.

TABLE I
Convergence of Mean Centerline Velocity U_c, Bulk Velocity U_b (Mass Weighted as in [14]), Wall Shear Stress $\langle \mu \frac{du}{dy} \rangle_w$, and Shape Factor H

Grid	U_c	U_b	$\langle \mu \frac{du}{dy} \rangle w$	H
$12 \times 41 \times 12$	17.7	15.2	169.2	1.65
$24 \times 81 \times 24$	18.2	15.7	180.6	1.64
$36 \times 121 \times 36$	18.2	15.7	181.1	1.61
Incompressible	18.2	15.6	180.0	1.62

Note. The incompressible flow reference is from Kim *et al*. [17].

the $36 \times 121 \times 36$ fourth-order compressible simulation with a $32 \times 81 \times 32$ fully spectral incompressible simulation using the method described in [16]. Good agreement is found, as expected for this Mach number (0.1 based on friction velocity or 1.8 based on centreline velocity).

The convergence of various global measures is shown on Table I for the grids already discussed. For the pressure gradient and Reynolds number specified, the velocity gradient at the wall should be 180, with difference from this being an error of the simulation. Here Re_τ is the Reynolds number based on u_τ, the mean density at the wall $\langle \rho_w \rangle$ and the mean viscosity $\langle \mu_w \rangle$ at the wall. For the finest grid the resolution in wall units (a common check on resolution in DNS) is $\Delta_x^+ = 15$ and $\Delta_z^+ = 7.5$ and approximately 10 point are in the sublayer $y^+ < 10$. The simulations demonstrate a robustness down to very coarse resolutions, comparable with the best incompressible turbulent flow solvers incorporating dealiasing and skew-symmetric formulation of the convective terms.

6. COMPARISON WITH COLEMAN *ET AL.*

Coleman *et al*. [14] carried out comparable simulations in their study of the effects of Mach number on turbulence statistics. In this section we simulate their case $Re_\tau = 190$ and $M_\tau = 0.095$. In this case the uniform body force term (36) was used together with variable fluid properties (power-law temperature dependence of the viscosity with exponent 0.7 and fixed Prandtl number $Pr = 0.7$). With the variable viscosity there is a need to use a larger computational box size than was used in the previous section, since turbulence structures become larger as the viscosity is reduced (the wall is cold relative to the bulk flow). We chose to use a box of size $6 \times 2 \times 3$, i.e., twice as large in x and z as in the previous section. This size is still somewhat lower than Coleman *et al*., who used a box of size $4\pi \times 2 \times 4\pi/3$. A computational grid of $60 \times 141 \times 60$ was used, giving $\Delta x^+ = 19$ and $\Delta z^+ = 9.5$, which

TABLE II
Comparison of Centerline Velocity U_c, Bulk Velocity U_b, Wall Shear Stress $\langle \mu \frac{du}{dy} \rangle_w$, and Shape Factor H with Those of Coleman *et al.* [14]

Simulation	U_c	U_b	$\langle \mu \frac{du}{dy} \rangle_w$	H
Current	18.9	16.3	190.3	1.66
Coleman *et al.*	18.5	15.9	189.5	1.65

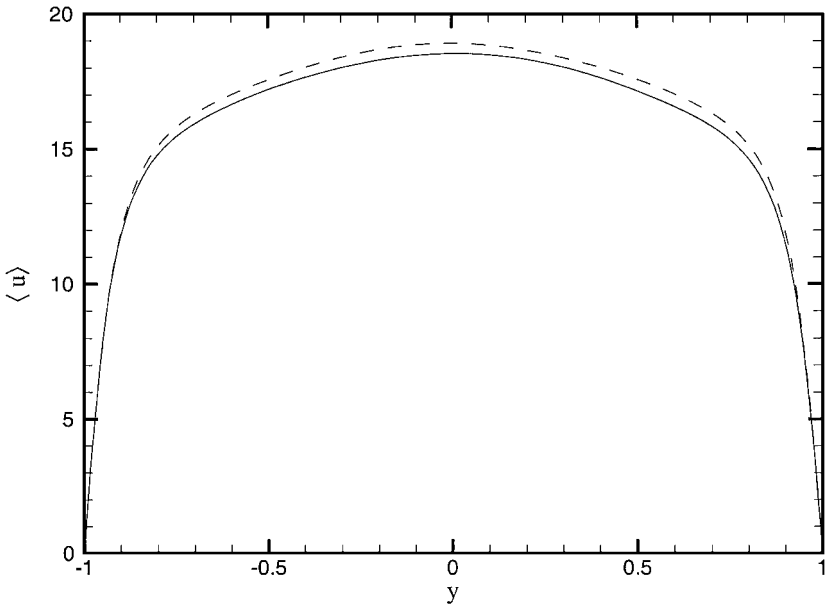

FIG. 5. Mean-velocity profile, comparing current simulation (dashed line) with that of Coleman *et al*. [14] (solid line).

are comparable to those used by Coleman *et al*. (16.6 and 10.0, respectively). There were 12 points in the sublayer ($y^+ < 10$).

For this simulation a parallel implementation was used, which incidentally illustrated the excellent parallel scaling of the method on a Cray T3E-1200E computer (90% efficiency

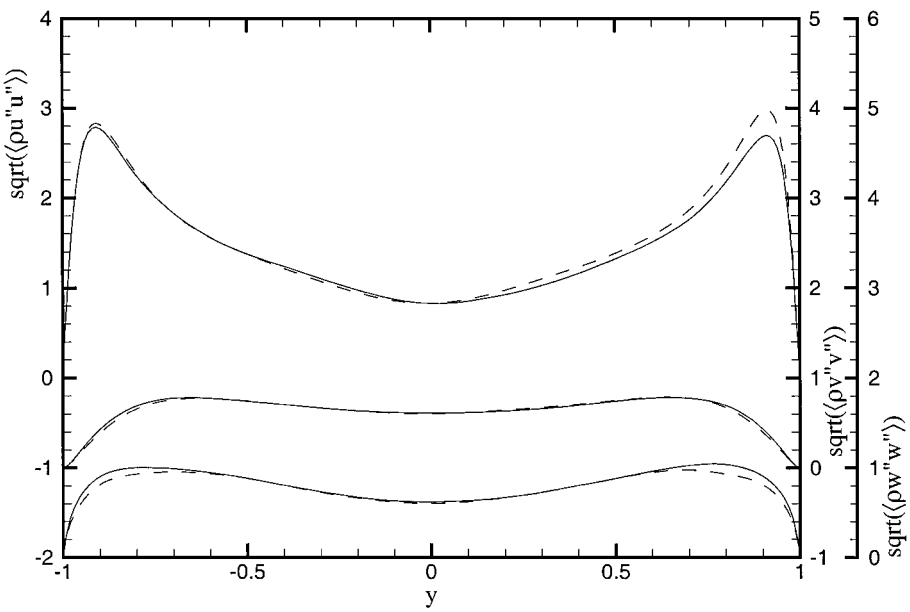

FIG. 6. Root mean normal turbulent stresses, comparing current simulation (dashed line) with that of Coleman *et al*. [14] (solid line). The top curves relate to the left scale, the middle to the right scale, and the lowest to the furthest right scale.

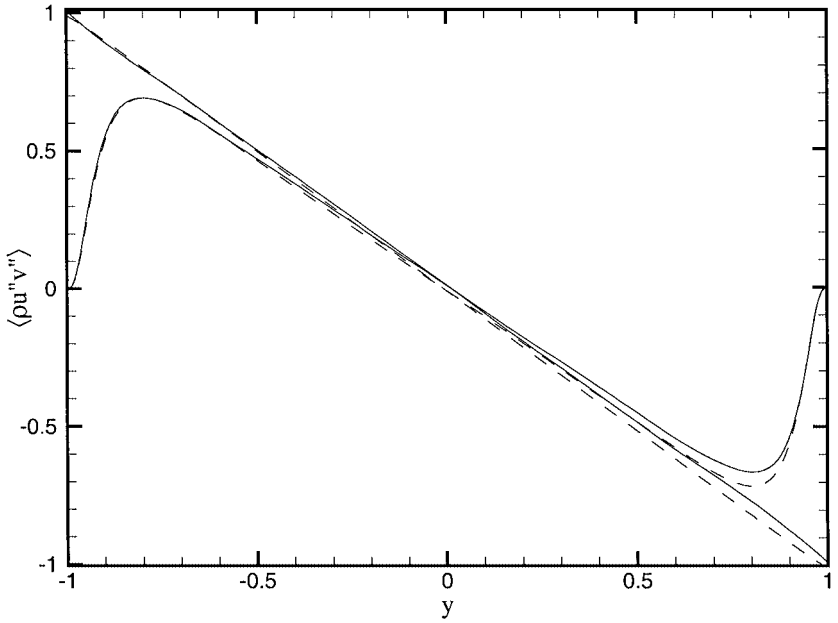

FIG. 7. Turbulent and total shear stresses, comparing current simulation (dashed line) with that of Coleman *et al*. [14] (solid line).

for a 240^3 benchmark on 256 processors and continued good scaling up to 768 processors, as reported in Ashworth *et al*. [19]). The simulation presented here used 32 processing elements.

Table II shows summary output from the simulation. Data from Coleman *et al*. have been renormalized to compare with the current simulation results. Figure 5 shows the mean-velocity profile, while Figs. 6 and 7 show the shear stress and rms turbulence fluctuations. Overall a good agreement is obtained, illustrating the good performance of the method for a resolution comparable to that of a spectral method. Good turbulence kinetic energy budgets have also been obtained [18].

7. DISCUSSION AND CONCLUSIONS

We have demonstrated how a numerical scheme for the compressible Navier–Stokes equations may be constructed that does not require filtering, upwinding, or additional viscosity to be stable for shock-free compressible turbulence computations. In this respect the method emulates the performance of the best incompressible flow formulations, which may use dealiasing, skew-symmetric formulation, or energy conservation (e.g., variables on a staggered grid) to obtain a robust method. The assessment of this performance is based on numerical tests on a low Mach number and Reynolds number compressible turbulent channel flow, and the accuracy comparison of the present scheme with the fifth-order WENO scheme (Hadjadj, private communication, 2000). For the same problem, the fifth-order WENO scheme is over six times more expensive yet more diffusive than the present scheme using the same temporal discretization. Without the use of the entropy splitting of the inviscid flux derivatives and Laplacian right hand side formulation, using the same CFL number, the solutions typically blow up before meaningful turbulence statistics can be obtained.

It is noted that, for this well-studied problem with accurate turbulent flow databases for comparison, we can safely conclude that entropy splitting in conjunction with the Laplacian formulation calculations were able to obtain stable fairly accurate solutions using coarse-to-moderate grid sizes without added numerical dissipation or filters. For problems that are less known, as with any approach and numerical method, one must know the limitation of the approach and exercise caution. Otherwise the methods may give an answer that is incorrect when low resolution is used, (see Yee and Sweby [20] for an example).

The numerical methods are currently being applied to several practical problems. Alam and Sandham [21] have studied shock-free transition to turbulence near the leading edge of aerofoil, while Lawal and Sandham [22] have used the above method in conjuction with shock-capturing schemes from Yee *et al*. [1] to study transitional shock boundary layer interaction in flow over a bump. These practical applications have been run without the need for changes to the numerical method and hence are leading to some confidence that the developments presented here are generally applicable for direct numerical simulation of compressible turbulent flow.

Several options remain for improving the capability of the method. Our numerical experiment employs a fully explicit time integrator. Perhaps a fully implicit [1, 5] or semiimplicit procedure might permit a more efficient (larger time step) time integration without sacrificing accuracy. For example, if acoustic and viscous terms could be made implicit it is estimated that a time step six times as large as that used for the simulations presented here could be used. Thus, the cost of any implicit treatment cannot be more than six times that of an explicit time step, or else no gain will be made. This is a fundamental problem for turbulent flow that must be computed in a time-accurate manner. The selection of an efficient and highly accurate temporal discretization is a subject of future research.

A further step in this work will be to couple the entropy splitting and Laplacian formulation discussed here with recent improvements [2–4] to the Yee *et al*. [1] schemes for simulations of shock-turbulence interaction. For this type of flow the automatic switching on or off of both the specialized filter and the entropy splitting appears to be very promising. In addition, a study will be made of the potential benefits of sixth-order differencing schemes over the fourth-order schemes considered here. In [1, 5] it was found that while the sixth-order scheme required slightly more operations count, it was more accurate than the fourth-order scheme. We would like to point out that the Carpenter *et al*. boundary scheme for the sixth-order interior scheme is not very stable. On the other hand, the Strand grid stencil for a stable boundary difference operator associated with the sixth-order interior scheme is two points wider than the Carpenter *et al*. variant for the same interior scheme. In this case, we have to use the boundary scheme starting at the eighth point from the physical boundaries. However, the sixth-order scheme may out-perform its fourth-order counterpart, since the slight increase in CPU required may well be compensated for by the gain in accuracy and, as a consequence, the possibility of using a coarser grid.

ACKNOWLEDGMENTS

The authors thank M. Vinokur of NASA Ames Research Center for numerous discussions on the theoretical development of entropy splitting and for help in checking the computer code implementation. Special thanks to T. J. Coakley of NASA Ames Research Center for his critical review of the manuscript and to Dr. G. N. Coleman for providing the channel flow data and for numerous discussions. This work has been supported in part by RIACS of NASA Ames Research Center. The first author would like to acknowledge additional support from EPSRC under Grants GR/M 21546 and GR/M 84336.

REFERENCES

1. H. C. Yee, N. D. Sandham, and M. J. Djomehri, Low dissipative high order shock-capturing methods using characteristic-based filters, *J. Comput. Phys.* **150**, 199 (1999).
2. B. Sjögreen and H. C. Yee, *Multi-Resolution Wavelet Based Adaptive Numerical Dissipation Control for Shock-Turbulence Computations*, RIACS Technical Report (NASA Ames Research Center, 2000).
3. H. C. Yee and B. Sjögreen, Designing adaptive low-dissipative high order schemes for long-time integrations, in *Turbulent Flow Computation*, edited by D. Drikakis and B. Geurts (Kluwer, 2002).
4. Deleted in proof.
5. H. C. Yee, M. Vinokur, and M. J. Djomehri, Entropy splitting and numerical dissipation, *J. Comput. Phys.* **161**, 1 (2000).
6. P. Olsson and J. Oliger, *Energy and Maximum Norm Estimates for Nonlinear Conservation Laws*, RIACS Technical Report 94-01 (NASA Ames Research Center, 1994).
7. M. Gerritsen and P. Olsson, Designing an efficient solution strategy for fluid flows. I. A stable high order finite difference scheme and sharp shock resolution for the Euler equations, *J. Comput. Phys.* **129**, 245 (1996).
8. M. Vinokur and H. C. Yee, Extension of efficient low dissipation high order schemes for 3-D curvilinear moving grids, in *Proceedings of the Computing the Future. III: Frontiers of Computational Fluid Dynamics-2000, June 26–28, Half Moon Bay, CA*, NASA/TM-2000-209598.
9. A. Harten, On the symmetric form of systems of conservation laws with entropy, *J. Comput. Phys.* **49**, 151 (1983).
10. B. Strand, Summation by parts for finite difference approximations for d/dx, *J. Comput. Phys.* **110**, 47 (1994).
11. P. Olsson, *Summation by Parts, Projections and Stability,* RIACS Technical Report (NASA Ames Research Center, 1994–1995).
12. M. H. Carpenter, J. Nordstrom, and D. Gottlieb, *A Stable and Conservative Interface Treatment of Arbitrary Spatial Accuracy, J. Comput. Phys.* **148**, 341 (1999).
13. N. D. Sandham and H. C. Yee, Entropy splitting for high-order numerical simulation of compressible turbulence, in *Proceedings of First International Conference on Computational Fluid Dynamics, Kyoto, Japan, July 10–14, 2000*, edited by N. Satofuka (Springer, 2001).
14. G. N. Coleman, J. Kim, and R. Moser, A numerical study of turbulent supersonic isothermal-wall channel flow, *J. Fluid Mech.* **305**, 159 (1995).
15. P. G. Huang, G. N. Coleman, and P. Bradshaw, Compressible turbulent channel flows: DNS results and modeling, *J. Fluid Mech.* **305**, 185 (1995).
16. N. D. Sandham and R. J. A. Howard, Direct simulation of turbulence using massively parallel computers. in *Parallel Computational Fluid Dynamics*, edited by D. R. Emerson, *et al.* (Elsevier, Amsterdam/New York, 1998).
17. J. Kim, P. Moin, and R. D. Moser, Turbulence statistics in fully-developed channel flow at low Reynolds number, *J. Fluid Mech.* **177**, 133 (1987).
18. Q. Li, *Direct Numerical Simulation of Compressible Turbulent Channel Flow*, Ph.D. thesis. (University of Southampton, 2002), in preparation.
19. M. Ashworth, D. R. Emerson, N. D. Sandham, Y. F. Yao, and Q. Li, Parallel DNS using a compressible turbulent channel flow benchmark, in *Proc. ECCOMAS CFD Conference, Swansea, Wales, 4–7 Sept. 2001.*
20. H. C. Yee and P. K. Sweby, *Dynamics of Numerics & Spurious Behaviors in CFD Computations*, RIACS Technical Report 97.06 (NASA Ames Research Center, 1997).
21. M. Alam and N. D. Sandham, DNS of transition near the leading edge of an aerofoil, in *Direct and Large-Eddy Simulation IV*, edited by B. J. Geurts, R. Friedrich, and O.Métais (Kluwer Academic, Dordrecht/New york, 2001).
22. A. A. Lawal and N. D. Sandham, Direct simulation of transonic flow over a bump, in *Direct and Large-Eddy Simulation IV*, edited by B. J. Geurts, R. Friedrich, and O.Métais (Kluwer Academic, Dordrecht/New york, 2001).